scientific reports

Check for updates

OPEN

Unraveling the molecular basis of membrane-associated release of coxsackievirus B3

Rodrigo Arce[1,2,3]✉, Martín Soñora[4], Iván Andreu-Moreno[1], Pilar Moreno[2,3], Gonzalo Moratorio[2,3] & Rafael Sanjuán[1]✉

Coxsackievirus B3 (CVB3), a member of the Enterovirus genus within the *Picornaviridae* family, has emerged as a key model for studying viral evolution and pathogenesis. Although traditionally considered obligate lytic viruses, recent research reveals that enteroviruses can also be released non-lytically within extracellular vesicles (EVs). This study explores the impact of mutations at position 63 of the VP3 capsid protein on CVB3 fitness and release mechanisms by substituting asparagine at this position with aromatic, charged, and aliphatic amino acids. We show that mutations at position 63 significantly affect viral release mechanisms and viral spread in cell culture. Specifically, aromatic mutations (N63H, N63Y, N63F, N63W) and the N63D mutation reduce the release of membrane-associated viral particles, while aromatic residues increase viral spread in cell culture and plaque size under specific conditions. These findings suggest that N63 mutations alter protomer interactions, influencing viral release, spread, and plaque formation, providing insights into the molecular mechanisms of CVB3 egress.

Keywords Coxsackievirus B3, Viral release, Viral spread, Plaque size, Enteroviruses

Enterovirus constitute a large and diverse genus within the family *Picornaviridae*. Although enteroviruses have traditionally been described as naked and obligate lytic viruses[1], it has been more recently shown that they can be released non-lytically in association with membranes, usually within extracellular vesicles (EVs) containing pools of viral particles or RNA. This alternative egress mode has been demonstrated in poliovirus, rhinovirus A, coxsackievirus B3 (CVB3), and coxsackievirus B1[2–5] but also in other picornaviruses such as hepatitis A virus, food-and-mouth disease virus, and encephalomyocarditis virus[6–8], as well as other non-enveloped viruses such as hepatitis E virus[9], astroviruses[10], and rotaviruses[11]. It has been suggested that membrane-associated viral release plays a role in enterovirus biology by enhancing infectivity, promoting immune evasion, and pathogenesis[4,6,8,12–14].

CVB3 has become a preferred enterovirus model, since poliovirus is less used in research due to efforts towards its eradication. Our group has previously investigated the release of membrane-associated particles in CVB3[15]. Specifically, experimental evolution revealed that substitution of asparagine at residue 63 of VP3 with histidine (N63H) drastically reduces this egress mode. N63 mutations have been independently identified and found to increase CVB3 fitness in other viral evolution studies[15–19]. N63H increases the efficiency of viral spread in HeLa cells, producing a large-plaque phenotype, a characteristic also observed when N63 is substituted with tyrosine (N63Y)[18].

The N63 position of VP3 in the CVB3 capsid protomer is centrally located on the external side and may interact with a tyrosine at position 173 in VP2 (Y173) (Fig. 1). This led us to hypothesize that VP3 mutations N63H and N63Y might enable Pi-stacking with Y173, altering the interaction between VP2 and VP3 and providing a potential mechanistic basis for the observed phenotypes. Based on the physical-chemical properties of these amino acids, we predicted that other residues with an aromatic side chain at N63 should produce phenotypes similar to those of the N63H and N63Y mutants. Here we test this hypothesis by characterizing the membrane-associated release, plaque size, and fitness of several N63 mutants.

[1]Virus Evolution Laboratory, Institute for Integrative Systems Biology (I2SysBio), Universitat de València-CSIC, Paterna, Spain. [2]Molecular Virology Laboratory, Center for Nuclear Research, Faculty of Sciences, Universidad de la República, Montevideo, Uruguay. [3]Experimental Evolution of Viruses, Institut Pasteur de Montevideo, Montevideo, Uruguay. [4]Biomolecular Simulations Group, Institut Pasteur de Montevideo, Mataojo 2020, Montevideo 11400, Uruguay. ✉email: rodrigo.arce@uv.es; rafael.sanjuan@uv.es

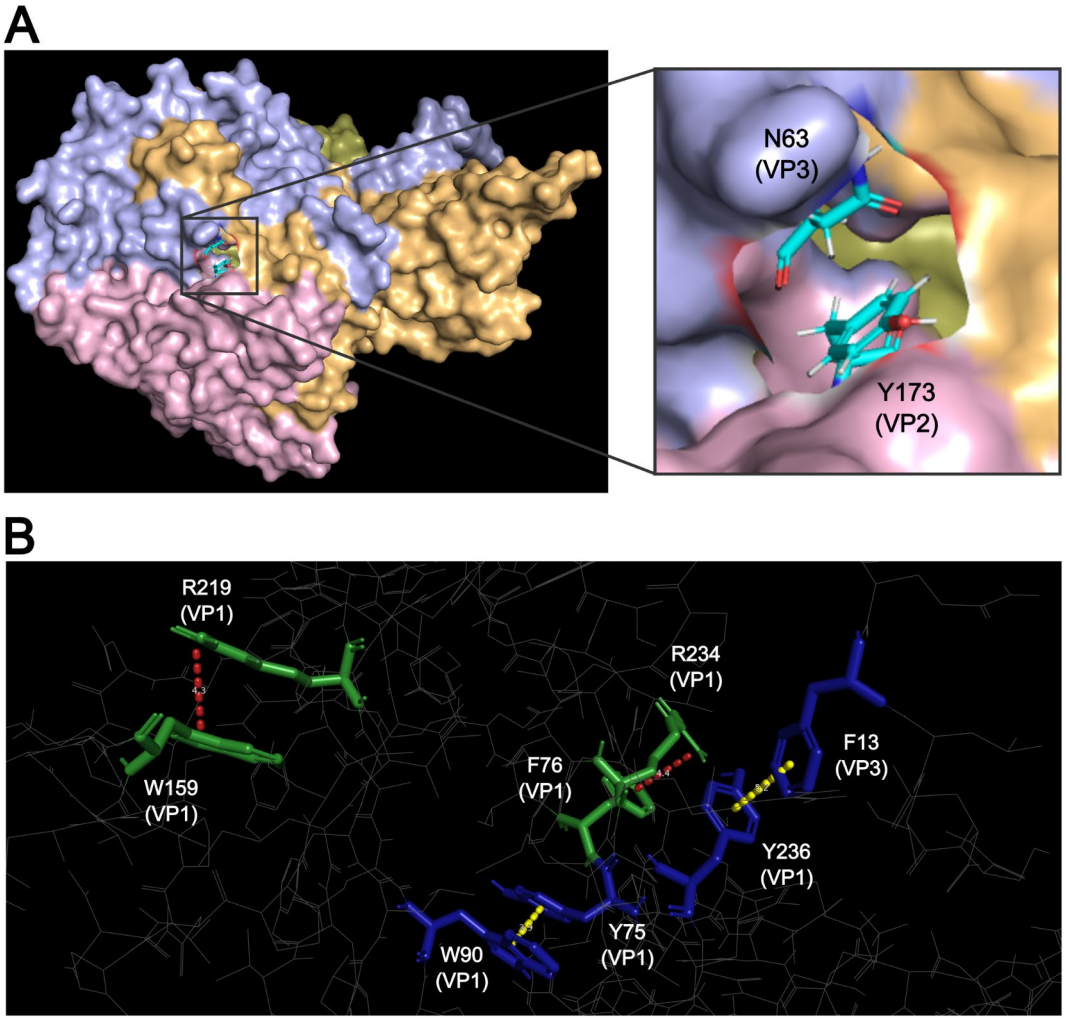

Fig. 1. Structural analysis of coxsackievirus B3 protomer (PDB: 1COV) highlighting the residue N63 and the possible interactions involved with Y173. All the images were generated using the PyMOL Molecular Graphics System, Version 3.0.5 Schrödinger, LLC. (**A**) Cartoon representation of the viral protomer showing VP1 (orange), VP2 (red), VP3 (blue), and VP4 (yellow). The inset focuses on residue N63 of VP3 and its proximity to Y173 of VP2. (**B**) Interactions of amino acids between and with aromatic rings in CVB3 protomer. Blue residues are involved in Pi-stacking interactions (yellow dashed lines), while green residues are involved in Pi-cation interactions (red dashed lines).

Results

Relevance of N63 in genus *Enterovirus*

To understand the importance of this residue in a broader context, we performed a sequence analysis of 281 members of the genus *Enterovirus* (Additional file 1: Table S1) with a complete sequence in NCBI. A previous work described the conservation of this residue in coxsackieviruses and echoviruses[18], particularly among members of the species *Enterovirus B* (coxsackievirus B1, coxsackievirus B3, enterovirus B97, enterovirus B, echovirus E30, echovirus E6) and *Enterovirus C* (coxsackievirus A1). After aligning all these sequences, our results indicate that asparagine (N) is the most frequent amino acid at this position in our sequence analysis (29.5%; Fig. 2), although its frequency is variable among species.

Residue N63 determines viral release in membrane-associated complexes

We introduced mutations N63H, N63Y, N63F, N63W, N63D, and N63L in a CVB3 Nancy infectious clone encoding for a mCherry reporter, and measured the percentage of viral particles released as membrane-associated complexes following a previously established protocol[4,15]. Briefly, we inoculated HeLa H1 cells at a multiplicity of infection (MOI) of 10 foci forming units (FFU) per cell. At 10 h post-inoculation (hpi), the culture supernatant was collected and centrifuged to remove debris. Then centrifuged again at a higher speed and the clarified supernatant obtained after this step was designated as the S fraction, whereas the pellet was resuspended and treated with detergent to disrupt lipid membranes (bP fraction). The ratio bP/(bP + S) is an indicator of the percentage of viral progeny released as membrane-associated complexes[15]. This ratio was 19.3 ± 4.4% for the non-mutated N63 virus (WT), whereas the aromatic (N63H, N63Y, N63F, N63W) and N63D mutants

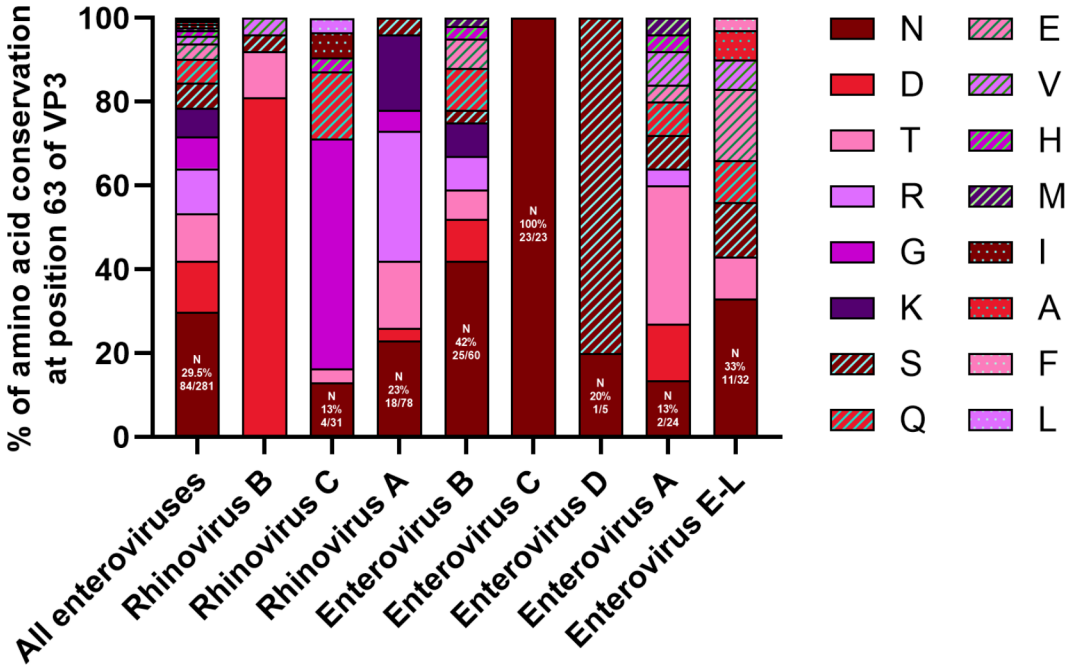

Fig. 2. Amino acid conservation at position 63 of VP3 protein across the genus *Enterovirus*. The bar chart represents the percentage of sequences with specific amino acids at this position for different species within the genus *Enterovirus*. Conservation values for asparagine (N) are expressed as a percentage, with the corresponding number of sequences analyzed indicated within each bar.

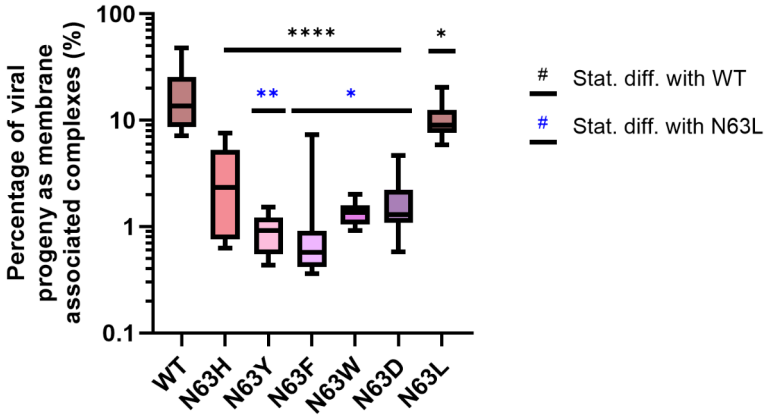

Fig. 3. Membrane-associated release of N63 mutants. Boxplot showing the percentage of viral progeny released as detergent-sensitive high-weight complexes, (bP/(bP + S). See text for details. Statistically significant differences between WT and mutants are indicated with black lines and symbols, while the differences between N63L and other mutants are indicated with blue symbols. *$P < 0.05$, **$P < 0.01$, ****$P < 0.001$ (one-way ANOVA with Tukey´s multiple comparison test).

showed significantly reduced values (one-way ANOVA with Tukey's multiple comparison test: $P < 0.05$; Fig. 3). These results suggest that specific mutations in residue 63 of VP3 can significantly affect viral progeny release, including all changes to aromatic side chains, but also the N63D substitution.

Aromatic residues at position N63 increase viral spread in cell culture

We next assessed the ability of these viruses to spread in cell culture. We inoculated HeLa H1 cells at an MOI of 0.001 FFU/cell and monitored infection spread using quantitative real-time fluorescence microscopy (Fig. 4). While no differences were detected during the initial infection cycle (approximately < 8 hpi[20]), indicating equal input, viral spread was faster for mutants with aromatic amino acids than the WT virus, N63D, and N63L mutants. Differences became maximal at 18–21 hpi, when mutants with aromatic amino acids infected twice as many cells as the WT, N63D, and N63L viruses (one-way ANOVA: $P < 0.001$). Viral spread started to plateau at the endpoint (24 hpi) and all viruses regained a similar final number of infected cells.

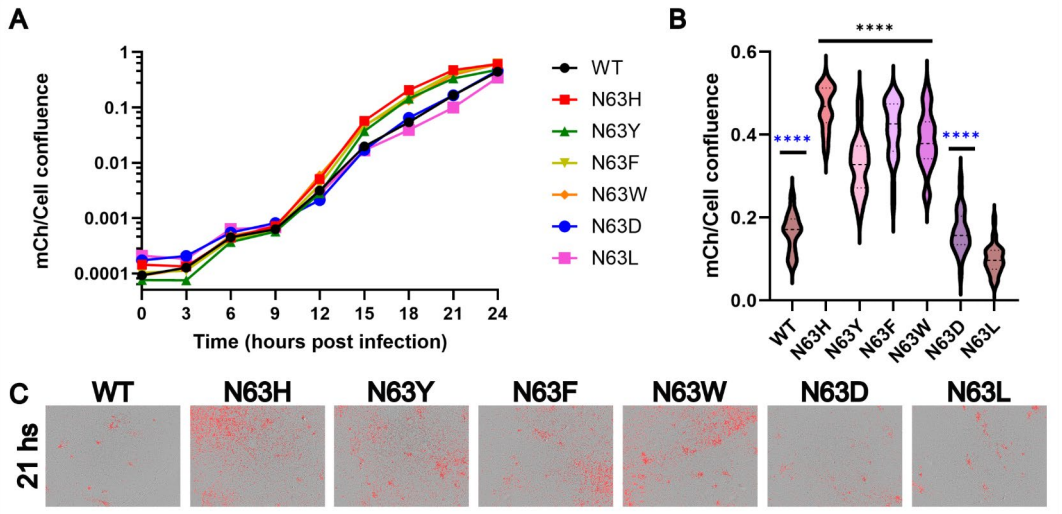

Fig. 4. Effect of N63 mutations on viral spread. (**A**) Growth curves of the non-mutated CVB3 (WT) and mutants N63H, N63Y, N63F, N63W, N63D, and N63L. Viral spread was monitored by measuring mCherry fluorescence at various time points post-inoculation. (**B**) Violin plot comparing mCherry signal at 21 hpi for WT and N63 mutants. Significance levels are represented as follows: ****$P < 0.0001$ (one-way ANOVA with Tukey´s multiple comparison test). Significant differences between WT and mutants are indicated with black lines and symbols, while the differences between N63L and other viruses are indicated with blue symbols. (**C**) Representative images showing the progression of infection in cells infected with WT and N63 mutants at 21 hpi.

Aromatic residues at position N63 selectively increase plaque size in agarose-containing medium

Standard plaque assays in agar semi-solidified medium revealed larger plaques for aromatic mutants compared to the WT, N63D and N63L viruses (one-way ANOVA: $P < 0.001$), consistent with the above results showing increased viral spread for these mutants. Agar is a mixture of agarose and agaropectin, a sulfated glycan. Because sulfated glycans can be attachment factors for viruses, they may affect plaque formation, and previous work found that the WT virus and N63Y mutant had different plaque phenotypes when agarose was used instead of agar[18,21]. Therefore, we performed plaque assays for all our viruses using agar and agarose and we compared the size of the plaques under each condition (Fig. 5). Some of the mutants with the aromatic amino acids (N63H, N63Y, N63F) and N63D showed significantly increased plaque size when agarose was used instead of agar (one-way ANOVA: $P < 0.001$). The strongest change corresponded to mutant N63D, with a fold increase of 7.2 ± 0.9. This increase was 1.4 ± 0.1 for the N63W mutant whereas, in contrast, the WT and N63L plaques were larger in agar than in agarose (fold changes of 0.50 ± 0.05 and 0.74 ± 0.09, respectively).

Molecular dynamics of CVB3 protomer and mutants at N63 position

After seeing these phenotypic differences between WT and mutants, we tried to investigate the structural implications of the mutations at residue N63 of VP3 in the viral protomer by performing molecular dynamics simulations (MDs) using a coarse-grain approach. We chose this strategy due to computational time constraints and because it allowed us to study protomer stability and flexibility over extended time scales, providing preliminary insights into the effects of mutations on the structural dynamics of the viral capsid. We conducted 5 µs MDs on the viral protomer of the WT virus and the six mutants (N63H, N63Y, N63F, N63W, N63D, N63L). Our analysis focused on evaluating viral protein stability through the analysis of several physical descriptors such as root mean square deviation (RMSD), radius of gyration (Rg), root mean square fluctuation (RMSF), solvent-accessible surface area (SASA), and the conservation and accuracy of the native contacts (Fig. 6). In all cases, the protomers were stable during the last 2 µs of simulation. The WT, N63W and N63F protomers displayed the highest stability, with RMSD values stabilizing around 1 Å during the last 2 µs. In contrast, N63H and N63Y exhibited higher RMSD values (> 1.2 Å) over the same time period, suggesting more significant conformational shifts. The compactness of the CVB3 protomer was assessed by analyzing the radius of gyration (Rg) over the simulation time. The mutant N63F exhibited the highest compactness with Rg values around 2.95 nm. Conversely, mutants N63H and N63Y showed more expanded structures, with Rg values reaching 3.15 nm, indicating a loss of structural compactness. RMSF profiles provided insights into the flexibility and amino acid residue fluctuations of specific regions across the VP1-VP4 proteins, and suggested that some mutants (N63H, N63Y, N63F and N63D) showed fluctuations along VP4, VP2 and VP1, which could lead to the destabilization of these regions. SASA analysis was focused on key residues VP2-Y173 and position 63 of VP3. Exposure of the VP2 Y173 residue was seen only for the N63D mutant, whereas VP3 N63 exposure was found for mutants N63D, N63F, N63L and N63Y, but not for mutants N63H, N63W and the WT.

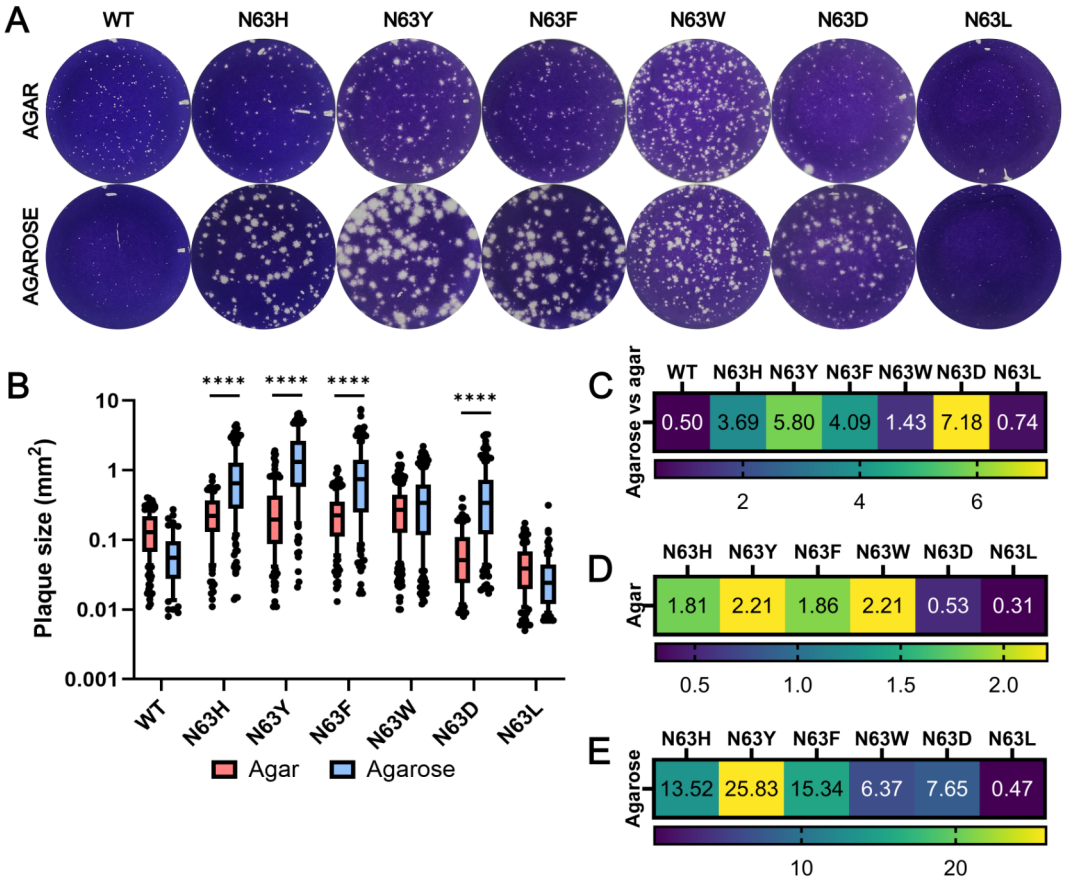

Fig. 5. Plaque phenotypes of N63 mutants in overlays of agar and agarose at 48 hpi. (**A**) Images of plaque assays performed with agar and agarose. (**B**) Boxplot comparing the plaque sizes (in mm^2) for each virus under each condition. The red boxes represent plaque sizes on agar, while the blue boxes represent plaque sizes on agarose. $^{****}P < 0.0001$ (one-way ANOVA with Tukey´s multiple comparison test). (**C**) Heat map showing the ratio of plaque sizes on agarose to those on agar for each virus. (**D**) Heat map comparing plaque sizes on agar relative to WT virus. (**E**) Heat map comparing plaque sizes on agarose relative to WT virus.

Discussion

Our results collectively suggest that aromatic amino acids at position 63 of the VP3 protein reduce association with membrane structures during viral egress and accelerate viral spread in cell culture, extending our previous results obtained with the N63H mutant[15]. These observations could help to explain the systematic emergence of N63 mutants in cell culture and vivo reported in different studies over the last years[15–18]. Typical naked enterovirus particles are considerably smaller than virus-containing EVs (30 nm for individual viral particles versus an average of ca. 350 nm for autophagosome-like EVs[4]). This may allow faster diffusion of naked particles and thus accelerate the viral spread of the N63 mutants, which are preferentially released in this form. A study in which all possible single point mutations in the CVB3 capsid were produced by deep mutational scanning found that the three fittest capsid mutants were precisely N63H, N63Y and N63F, and that N63W was among the 1.2% of beneficial mutations[17]. In contrast, other authors reported a growth defect for N63Y in cell cultures using single-cycle growth assays[18]. This discrepancy may be due to the use of different cell lines, MOIs, or other differences in the experimental design and deserves further investigation.

Our sequence analysis reveals variable conservation of residue 63 in VP3 among different species within the genus Enterovirus. While asparagine (N) is fixed in *Enterovirus C* and frequent in *Enterovirus B* (42%), its occurrence is significantly lower in other species, and it is completely absent in *Rhinovirus B*. Interestingly, all enteroviruses known to be released in vesicles (poliovirus, coxsackievirus B1, CVB3, rhinovirus A2) retain the asparagine residue at position 63 of VP3. Our results and previous works[15,17] indicate that N63 mutants, particularly N63H and N63Y, loose EV association and display increased viral fitness in cell culture. However, egress in EVs might be advantageous in vivo. While there is already work investigating N63Y in mice[18], our in vitro results contrast with many of these findings. Therefore, we believe it would be interesting to perform new in vivo experiments to better understand the importance of N63 variants and the role of EV-associated viral egress. Furthermore, it might be interesting to study these mutations in the context of the previously mentioned members of the genus *Enterovirus*.

We also found that certain amino acids at position 63 may alter the interaction of viral particles with sulfated glycans, as suggested by the plaque size ratios in agarose versus agar-containing medium. While WT virus

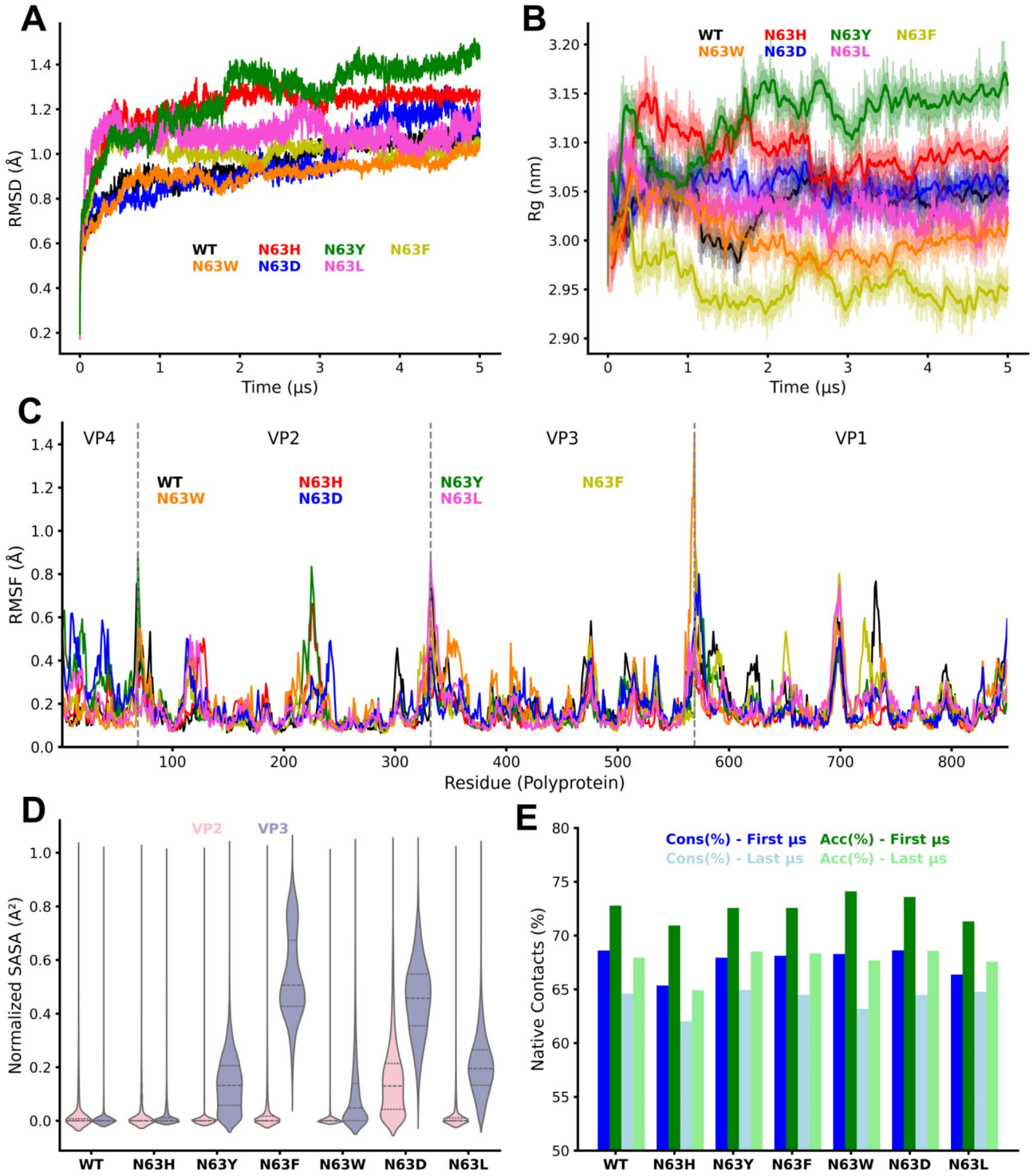

Fig. 6. Molecular dynamics simulations of CVB3 WT virus and mutants at VP3 residue N63. (**A**) RMSD of the capsid over 5 μs of the simulation. (**B**) Radius of gyration (Rg) over the time of the simulation. (**C**) RMSF per residue of the viral polyprotein. (**D**) Violin plot of SASA for VP2-Y173 (pink), and position 63 of VP3 (gray). (**E**) Percentage of native contacts (Cons%) and accuracy (Acc%) at the first and last microseconds of the simulation.

and N63L have smaller plaques in agarose compared to agar, the remaining mutants show the opposite. This difference is remarkable for most, but not all, of the aromatic amino acids, as well as for the N63D mutation. The exception to this difference between mutants that have larger plaques in agarose than in agar is N63W, which has a much larger plaque phenotype than WT virus in both conditions. Our results suggest that naked viral particles may have a higher affinity for sulfated glycans than membrane-enclosed particles. In contrast, previous work

with the N63Y mutant reported larger plaques with agar than with agarose[18]. Similar to our findings, studies with mengovirus, another picornavirus, found that the use of agarose or agar with glycosaminoglycan inhibitors produced larger plaques than agar alone[22].

MD simulations suggested changes in protomer compaction, stability, and solvent accessibility among N63 variants. However, the results of these simulations did not correlate with the experimental phenotypes. This discrepancy underscores the inherent limitations of coarse-grained simulations in capturing fine-grained molecular interactions. To address this issue, we propose as a future perspective to perform all-atom molecular dynamics simulations in triplicate. These simulations would provide a more detailed view of the interactions between the mutated residues and their surrounding amino acid environment.

A limitation of our work is that we did not characterize membrane-associated viral particles structurally or molecularly. These are typically complexes of multiple virions enclosed in large autophagosome-like EVs[4] and can therefore be readily separated from individual naked viral particles by slow-speed centrifugation[2,4]. However, these complexes can take additional forms and viral particles can also be packed into smaller vesicles[23]. Experiments should be performed to detect EV markers such as TSG101, CD9, CD63, or CD81[24], and EVs could be purified using gradient centrifugation.

Our results did not confirm the hypothesis that aromatic amino acids at VP3 position 63 may alter VP2-VP3 interactions, but are more consistent with effects related to the destabilization of the capsid. The exact mechanism producing the observed phenotypes remains thus unknown, and the capsid structural changes induced by these N63 mutations deserve future investigation. Functionally, N63 variants might alter the ability of the capsid to interact with membranes, but might also change the interaction of CVB3 with other autophagy components or endoplasmic reticulum-derived organelles. The mutants studied in this work could be an important tool to elucidate the mechanisms responsible for viral replication and release in association with membranes and EVs in CVB3, but also in other enteroviruses since N63 is a conserved residue between coxsackieviruses, echoviruses, and among members of the species *Enteroviruses C*. Future studies with these mutants could also investigate recombination events between different members of genus *Enterovirus* that utilize membrane-associated egress mechanisms, such as EVs. Since viral replication occurs on virus-induced membrane structures termed replication organelles[25], these shared membrane compartments may facilitate the close proximity of viral particles, enhancing genetic exchanges and thereby increasing recombination rates.

Methods

Cells and virus

HeLa-H1 cells were purchased from the American Type Culture Collection (ATCC, CRL-1958) and maintained in Dulbecco's modified Eagle's medium (DMEM) supplemented with 10% fetal bovine serum (FBS), non-essential amino acids, 10 units/ml penicillin, 10 mg/ml streptomycin, and 250 ng/ml amphotericin B, incubated at 37°C in a 5% CO_2 atmosphere. PCR tests confirmed that the cells were free from mycoplasma contamination. The Nancy mCherry-CVB3 virus and infectious clone were described in our previous work[2].

Site-directed mutagenesis

N63F, N63W, and N63L mutants were produced using the following primers: N63F For – 5'-GTTG GAGAGAA GGTCTTCTCTATGGAAGCATACC-3′; N63F Rev – 5′-GGTATGCTTCCATAGAGAAGACCTTCTCTCCA AC-3′; N63W For – 5′-GGAGAGAAGGTCTGGTCTATGGAAGCATACCAG-3′; N63W Rev – 5′-CTGGTA TGCTTCCATAGACCAGACCAGACCTTCTCTCC-3′; N63L For – 5′-GAGAGAAGGTCCTCTCTATGGAA GCATACC-3′; N63L Rev – 5′-GGTATGCTTCCATAGAGAGGACCTTCTCTC-3′. The CVB3 infectious clone was used as template for amplification with Phusion High-fidelity DNA Polymerase (ThermoScientific) under the following thermal profile: initial denaturation at 98°C for 1 min, 18 cycles of 95°C for 50 s, 50 s at 60°C, and 72°C for 7 min, followed by 7 min of final extension at 72°C. Products were digested with DpnI (ThermoScientific) at 37°C for 30 min to remove the methylated template. Then, these reactions were used to transform NZY5a competent cells (NZYTech) and the resulting colonies were sequenced (Plasmidsaurus) to confirm the success of mutagenesis, amplified, and used for plasmid extraction by the miniprep method. After confirmation, the plasmids were transfected in BHK T7 using Lipofectamine 3000 following the manufacturers indications. The supernatant was recollected, RNA was extracted and the success of the substitution was confirmed by Sanger sequencing. N63D and N63Y mutants were provided by Ron Geller. N63H was produced in our previous work.

Virus Titration by fluorescence microscopy

Confluent cells in 12 well plates were inoculated with 100 µL of virus supernatant in DMEM for 1 h. Cells were overlaid with 1 mL of culture medium containing 2% FBS and supplemented with 0.8% agarose. At 8 hpi, fluorescence imaging of cells was performed in an Incucyte SX5 Live-Cell Analysis System (Sartorius) kept in a humidified tissue culture incubator at 37°C and 5% CO_2. Images were captured with the 4X objective using phase contrast and the red channel.

Plaque size measurement

In the previous day to the assay, 6-well plates were seeded with 0.5×10^6 cells per well. On the day of the experiment, 200 µL of a countable viral dilution was inoculated in each well for 1 h. After inoculation, a semisolid medium was added to the monolayer. At 48 hpi cells were fixed by adding 2 ml of 10% formaldehyde to each well for 15 min and stained with 2% crystal violet in 10% formaldehyde for 10 min. Pictures of wells were analyzed with Fiji (ImageJ) for plaque size measurement.

Estimation of the percentage of viral progeny released as membrane-associated complexes

HeLa-H1 cells were inoculated with CVB3 in 12-well dishes at high MOI (10 FFU/cell) and after 1 h incubation the inoculum was removed, and DMEM supplemented with 2% FBS and 10 units/mL penicillin, 10 mg/mL streptomycin and 250 ng/mL amphotericin B was added. At 10 hpi, the supernatant was collected and centrifuged at 1000 g for 5 min at 4°C to remove large debris. The supernatant of this initial spin was collected and centrifuged at 15,000 g for 15 min at 4°C. The supernatant of this second centrifugation was stored until use at 4°C as the S fraction, whereas the pellet was resuspended and spun again under the same conditions to remove remaining free viral particles. This step was repeated twice and the third pellet was resuspended in 60 µL (P fraction). Membranes were disrupted (bP fraction) by adding 10 µL of 0.16% Triton X-100 to 50 µL of P fraction and incubating 30 min at 4°C. The S and bP fractions were titrated, and the bP/(bP + S) titer ratio was used to estimate the fraction of viral progeny released in the form of membrane-associated complexes. These assays were performed in triplicate.

Viral growth assays

Virus infections were carried out in HeLa-H1 monolayers cultured in 12-well plates and inoculated in triplicate with 100 µL at an MOI of 0.001 FFU/cell. Cells were incubated for 1 h, the inoculum was removed, cells were washed with PBS 1x, 1 mL of DMEM supplemented with 2% FBS was added, and cultures were incubated for 24 h. Viral infection was evaluated by fluorescence imaging every 3 h in the Incucyte SX5 Live-Cell Analysis System (Sartorius).

Molecular dynamics simulations of CVB3 mutants

The initial models for MD were based on the crystal structure of the CVB3 protamer from the pentameric virion, available in the Protein Data Bank (PDB ID: 1COV). Mutant variants were created through homology modeling using MODELLER[26] to generate structures with appropriate residue substitutions. These models were then refined to optimize side-chain conformations and overall structural quality in preparation for the simulations. The protomer models were based on the refined CVB3 X-ray diffraction structure at a resolution of 3.5 Å. Missing side-chain atoms and protons were added using pdb2pqr[27] at pH 7.0 to ensure structural completeness. A 5000-step energy minimization in vacuum was performed for each model using the AMBER 14SB force field to resolve steric clashes and eliminate unfavorable interactions. All MD simulations were performed using GROMACS (version 2018.4, https://www.gromacs.org/)[28], with the proteins and system represented using the coarse-grained SIRAH force field 2.0 to represent the proteins and the solvent models[29]. The system was solvated using the WT4 water model, with sodium and chloride ions added to neutralize the system and maintain a physiological ionic strength of 150 mM NaCl. A reference temperature of 300 K was maintained by separately coupling the solute and solvent to a V-rescale thermostat[30] with a coupling constant of 2 ps. Pressure was controlled at 1 bar using the Parrinello-Rahman barostat[31,32] with a coupling time of 8 ps. A minimum cutoff of 12 Å was used for non-bonded interactions, and long-range electrostatics were calculated using the Particle Mesh Ewald (PME)[33,34] method. Newton's equations of motion were integrated using a leapfrog algorithm with a time step of 2 fs for the first nanosecond, switching to 20 fs thereafter. Simulations were conducted for 5 µs, and snapshots were saved every 100 ps for analysis. RMSD was calculated to assess the overall stability of the system over time, using the Cα atoms and taking the experimental structure (PDB ID: 1COV) as the reference. RMSF values were computed for each residue to evaluate local flexibility, focusing on the last 1 µs of the trajectory. Rg was computed to assess the compactness of the viral protomers throughout the simulation. Variations in Rg values provide insights into the overall structural integrity and the extent of compaction or expansion of the viral capsid. SASA calculations were performed to determine the degree of exposure of protein residues to the solvent, with particular attention given to key residues (VP1 S266, VP2 Y173, VP3 N63) across all mutants. Non-covalent residue contacts were tracked throughout the simulations to evaluate the conservation of native contacts and any potential disruptions or new interactions caused by mutations. Contacts were monitored based on a distance cutoff of 8.0 Å between residue pairs. All visual representations of molecular structures and dynamics were generated using VMD[35]. RMSD, RMSF, Rg, SASA, and residue contact analyses were performed using the GROMACS[28] analysis package and homemade tcl scripts, allowing for a comprehensive evaluation of the structural dynamics of the CVB3 protomer and its mutants. All physical descriptors were plotted using homemade python scripts.

Data availability

The datasets used and/or analysed during the current study available from the corresponding author on reasonable request.

Received: 18 November 2024; Accepted: 26 February 2025
Published online: 10 March 2025

References

1. Lai, J., Sam, I. C. & Chan, Y. The autophagic machinery in enterovirus infection. *Viruses* **8**, 32 (2016).
2. Bou, J. V., Geller, R. & Sanjuán, R. Membrane-Associated enteroviruses undergo intercellular transmission as pools of sibling viral genomes. *Cell. Rep.* **29**, 714–723e4 (2019).
3. Jorfi, S. et al. A coxsackievirus B1-mediated nonlytic extracellular Vesicle-to-cell mechanism of virus transmission and its possible control through modulation of EV release. *J. Gen. Virol.* **104**, (2023).
4. Chen, Y. H. et al. Phosphatidylserine vesicles enable efficient En bloc transmission of enteroviruses. *Cell* **160**, 619–630 (2015).
5. Robinson, S. M. et al. Coxsackievirus B exits the host cell in shed microvesicles displaying autophagosomal markers. *PLoS Pathog.* **10**, e1004045 (2014).

6. Feng, Z. et al. A pathogenic picornavirus acquires an envelope by hijacking cellular membranes. *Nature* **496**, 367–371 (2013).
7. Zhang, K. et al. Exosomes-mediated transmission of foot-and-mouth disease virus in vivo and in vitro. *Vet. Microbiol.* **233**, 164–173 (2019).
8. van der Grein, S. G. et al. Picornavirus infection induces Temporal release of multiple extracellular vesicle subsets that differ in molecular composition and infectious potential. *PLOS Pathog.* **15**, e1007594 (2019).
9. Nagashima, S. et al. Hepatitis E virus egress depends on the Exosomal pathway, with secretory exosomes derived from multivesicular bodies. *J. Gen. Virol.* **95**, 2166–2175 (2014).
10. Baez-Navarro, C., Quevedo, I. R., López, S., Arias, C. F. & Iša, P. The association of human astrovirus with extracellular vesicles facilitates cell infection and protects the virus from neutralizing antibodies. *J. Virol.* **96**, (2022).
11. Iša, P., Pérez-Delgado, A., Quevedo, I. R., López, S. & Arias, C. F. Rotaviruses associate with distinct types of extracellular vesicles. *Viruses* **12**, 763 (2020).
12. Defourny, K. A. Y., Pei, X. & van Kuppeveld, F. J. M. Nolte-´t Hoen, E. N. M. Picornavirus security proteins promote the release of extracellular vesicle enclosed viruses via the modulation of host kinases. *PLOS Pathog.* **20**, e1012133 (2024).
13. Bou, J. V., Taguwa, S. & Matsuura, Y. Trick-or-Trap: extracellular vesicles and viral transmission. *Vaccines* **11**, 1532 (2023).
14. Fu, Y. & Xiong, S. Exosomes mediate coxsackievirus B3 transmission and expand the viral tropism. *PLOS Pathog.* **19**, e1011090 (2023).
15. Bou, J. V. & Sanjuán, R. Experimental evolution reveals a genetic basis for Membrane-Associated virus release. *Mol. Biol. Evol.* **38**, 358–367 (2021).
16. Mattenberger, F., Vila-Nistal, M. & Geller, R. Increased RNA virus population diversity improves adaptability. *Sci. Rep.* **11**, 6824 (2021).
17. Mattenberger, F., Latorre, V., Tirosh, O., Stern, A. & Geller, R. Globally defining the effects of mutations in a picornavirus capsid. *Elife* **10**, (2021).
18. Wang, Y. & Pfeiffer, J. K. Emergence of a Large-Plaque Variant in Mice Infected with Coxsackievirus B3. *MBio* 7, (2016).
19. Bordería, A. V. et al. Group selection and contribution of minority variants during virus adaptation determines virus fitness and phenotype. *PLOS Pathog.* **11**, e1004838 (2015).
20. Jiang, P., Liu, Y., Ma, H. C., Paul, A. V. & Wimmer, E. Picornavirus morphogenesis. *Microbiol. Mol. Biol. Rev.* **78**, 418–437 (2014).
21. Möller, S. et al. High-Sulfated glycosaminoglycans prevent coronavirus replication. *Viruses* **14**, 413 (2022).
22. Borden, E. C., Gary, G. W. & Murphy, F. A. Comparison of agar and agarose preparations for Mengovirus plaque formation. *Appl. Microbiol.* **20**, 289–291 (1970).
23. Yang, J. E. et al. Complexity and ultrastructure of infectious extracellular vesicles from cells infected by non-enveloped virus. *Sci. Rep.* **10**, 7939 (2020).
24. Welsh, J. A. et al. Minimal information for studies of extracellular vesicles (MISEV2023): from basic to advanced approaches. *J. Extracell. Vesicles* **13**, (2024).
25. Baggen, J., Thibaut, H. J., Strating, J. R. P. M. & van Kuppeveld, F. J. M. The life cycle of non-polio enteroviruses and how to target it. *Nat. Rev. Microbiol.* **16**, 368–381 (2018).
26. Šali, A. & Blundell, T. L. Comparative protein modelling by satisfaction of Spatial restraints. *J. Mol. Biol.* **234**, 779–815 (1993).
27. Jurrus, E. et al. Improvements to the APBS biomolecular solvation software suite. *Protein Sci.* **27**, 112–128 (2018).
28. Páll, S., Abraham, M. J., Kutzner, C., Hess, B. & Lindahl, E. Tackling exascale software challenges in molecular dynamics simulations with GROMACS. in 3–27 (2015). https://doi.org/10.1007/978-3-319-15976-8_1
29. Machado, M. R. et al. The SIRAH 2.0 force field: Altius, Fortius, Citius. *J. Chem. Theory Comput.* **15**, 2719–2733 (2019).
30. Bussi, G., Donadio, D. & Parrinello, M. Canonical sampling through velocity rescaling. *J. Chem. Phys.* **126**, (2007).
31. Nosé, S. & Klein, M. L. Constant pressure molecular dynamics for molecular systems. *Mol. Phys.* **50**, 1055–1076 (1983).
32. Parrinello, M. & Rahman, A. Polymorphic transitions in single crystals: A new molecular dynamics method. *J. Appl. Phys.* **52**, 7182–7190 (1981).
33. Darden, T., York, D. & Pedersen, L. Particle mesh Ewald: an N ·log(N) method for Ewald sums in large systems. *J. Chem. Phys.* **98**, 10089–10092 (1993).
34. Essmann, U. et al. A smooth particle mesh Ewald method. *J. Chem. Phys.* **103**, 8577–8593 (1995).
35. Humphrey, W., Dalke, A. & Schulten, K. VMD: visual molecular dynamics. *J. Mol. Graph.* **14**, 33–38 (1996).

Acknowledgements

This work was financially supported by an ERC Advanced Grant (101019724—EVADER) and a grant from the Spanish Ministerio de Ciencia e Innovación (PID2020-118602RB-I00—ZooVir) to R.S. We thank ANII (Agencia Nacional de Investigación e Innovación, Uruguay) for the grant MOV_CA_2021_1_171985 and CSIC (Universidad de la República, Uruguay) through Programa MIA for supporting R.A. during an internship at the Universitat de Valencia. This work was supported by FOCEM - Fondo para la Convergencia Estructural del Mercosur (COF 03/11) to M.S and the Institut Pasteur de Montevideo. We thank Natalia Echeverría for her helpful comments during the initial stages of the project and Jaime Buigues for helpful advises during the revision process.

Author contributions

Conceptualization: RA. Investigation: RA, RS. Data analysis: RA, MS, IAM. Funding: RS, GM, PM. Resources: RS. Writing: RA, RS.

Declarations

Competing interests

The authors declare no competing interests.

Additional information

Supplementary Information The online version contains supplementary material available at https://doi.org/10.1038/s41598-025-92289-x.

Correspondence and requests for materials should be addressed to R.A. or R.S.